Research Article

Junjun Shen*, Decheng Chen, Kongquan Chen, Yubing Ji, Pengwan Wang, Junjun Li, Quansheng Cai, and Jianghui Meng

Shale types and sedimentary environments of the Upper Ordovician Wufeng Formation-Member 1 of the Lower Silurian Longmaxi Formation in western Hubei Province, China

https://doi.org/10.1515/geo-2020-0320
received August 04, 2021; accepted November 20, 2021

Abstract: By performing scanning electron microscopy, microscopic observations, whole-rock X-ray diffraction analysis, organic geochemistry analysis, and elemental analysis on drill core specimens and thin sections, in this study, we classified the shale types of the Wufeng Formation-Member 1 of the Longmaxi Formation in western Hubei, southern China, and explored the development characteristics and formation environments of the different shale types. The results show that (1) the shales of the Wufeng Formation-Member 1 of the Longmaxi Formation are composed of three types of shale: siliceous shale, mixed clay-siliceous shale, and clay shale. The siliceous shale is a type of shale unique to deep-water environments; clay shale is the main type of shale formed in shallow-water environments; and mixed clay-siliceous shale falls between the two. (2) The changes in shale type are characterized by multiple depositional cycles in the vertical direction with strong heterogeneity and an obvious tripartite character, and the siliceous shales gradually thicken as they laterally extend northwestward, with their last depositional cycle gradually ending at a later time. (3) The Late Ordovician-Early Silurian paleoenvironment can be divided into six evolutionary stages (A, B, C, D, E, and F) from early to late. In particular, the sea level was relatively lower in stages A and F when the bottom water was mainly oxygen rich with higher terrigenous inputs and a lower paleoproductivity, which led to the formation of clay shales poor in organic matter but rich in terrigenous quartz clasts. The sea level was higher in stages B, C, and D when the bottom water was anoxic with lower terrigenous inputs and a higher paleoproductivity, which led to the formation of siliceous shales rich in organic matter and biogenic silica. The total organic carbon (TOC) contents of siliceous shales decrease in the order of stage C > stage D > stage B, which is mainly attributed to the different degrees of water restriction in the three stages and the consequently different paleoproductivities. Stage E corresponds to the mixed clay-siliceous shales, the depositional environment of which is between those of the siliceous shales and the clay shales, thereby resulting in the mineral composition and TOC content of the mixed clay-siliceous shales being between those of the other two shale types.

Keywords: Middle Yangtze, black shale, organic matter, paleoenvironment, depositional model

*** Corresponding author: Junjun Shen,** Hubei Cooperative Innovation Center of Unconventional Oil and Gas of Yangtze University, Wuhan 430100, Hubei, China, e-mail: shenhema@163.com
Decheng Chen: Jingzhou Institute of Technology, Jingzhou 434000, China
Kongquan Chen, Jianghui Meng: Hubei Cooperative Innovation Center of Unconventional Oil and Gas of Yangtze University, Wuhan 430100, Hubei, China
Yubing Ji: Zhejiang Oilfield Company Intergeration Center of Exploration & Development, Hangzhou 310000, Zhejiang, China
Pengwan Wang: PetroChina Hangzhou Institute of Petroleum Geology, Hangzhou 310023, Zhejiang, China
Junjun Li: PetroChina Zhejiang Oilfield Company, Hangzhou 310023, Zhejiang, China
Quansheng Cai: School of Geoscience, Yangtze University, Wuhan 430100, Hubei, China

1 Introduction

Earlier studies have suggested that shale formed in a specific environment is homogeneous without obvious structures, but shales with heterogeneous characteristics have been widely reported with the advancement of fine-grained sedimentology [1–3], and thus, it has been accepted that shale is composed of different types of rocks that are

rich in organic matter [4]. Given that shale lithofacies contain macroscopic and microscopic information such as color, sedimentary structure, and groundmass structure, as well as the inorganic and organic mineral compositions [5–7], shale lithofacies classification has become a basic geological tool in shale gas exploration. Furthermore, given the notion that "a depositional environment is the cause and a sedimentary rock is the result" [8], studies on the formation environments and development patterns of shales have also focused on the types of shale lithofacies [3]. Earlier studies have discovered that the differences in the mineral compositions, sedimentary structures, organic matter contents, and paleontological types and abundances of different types of rocks are the result of the combined action of the basin structure, water environment, terrigenous supply, climate change, and sea-level rise and fall during shale deposition [9–11]. Therefore, the classification of shale lithofacies and the research on shale depositional environments provide important guidance for determining the depositional conditions of black shales and for finding sweet spots in shale gas exploration.

The Wufeng Formation–Longmaxi Formation in western Hubei is characterized by a large thickness of organic-rich shale, with a high organic carbon content and high organic maturity, which serves as an important replacement area for shale gas exploration in southern China after the Sichuan Basin [12–14]. Earlier studies of this area have mainly focused on the tectonic background and shale gas preservation conditions [15,16], biostratigraphic classification and comparison [17,18], lithofacies paleogeography [19–21], and organic geochemistry [22], whereas relatively little research has been conducted on the characterization of the rock types. Moreover, the classification criteria for rock types has not been unified [14,23], and no systematic study has been conducted on the formation environments and development patterns of the different types of shales. Earlier studies have identified paleoproductivity and redox conditions as the key factors controlling the formation of different types of shales, but few have explored the impact of water restriction on shale formation, and much remains unknown about the correlation between environmental factors [10,13,14,24], thereby preventing the development of satisfactory shale deposition models for different shale types.

Given these issues, the black shales of the Upper Ordovician Wufeng Formation–Lower Silurian Longmaxi Formation in the western part of Hubei Province were selected as the research objects of this study. Scanning electron microscopy, thin section microscopic observations, whole-rock X-ray diffraction analysis, organic geochemistry analysis, and elemental analysis were performed to enable the detailed classification of the various types of marine shales. Based on the classification results, we clarified the development characteristics and temporal-spatial patterns of the different shale types, explored the formation environments of different shale types in terms of sea level variations, terrestrial inputs, redox conditions, paleoproductivity, and water restriction and established depositional evolution models. These findings deepen our understanding of the deposition and development mechanisms of marine shales and provide a theoretical basis for the identification of sweet spot layers in shale gas exploration in western Hubei.

2 Regional geologic background

The study area is geographically located in the western part of Hubei Province (Figure 1a), covering Yichang, Jingmen, and Nanzhang (Figure 1b). Since the Middle Ordovician, the Yangtze Plate ended its development as a passive continental margin and evolved into a foreland basin due to its convergence with the Cathaysia Block [25–27]. In the Late Ordovician–Early Silurian, as the collision and compression of the Cathaysia Block with the Yangtze Plate strengthened, the Jiangnan-Xuefeng uplift, the Central Guizhou uplift, the Kangdian uplift, and the Central Sichuan uplifts on the margin of the Yangtze Plate rapidly exposed the strata making it an ancient land. Meanwhile, underwater highlands were formed in some areas, thereby partially transforming the Yangtze region from an open sea into a confined sea in the Middle Ordovician, which created a large-area, low-energy, undercompensated, anoxic depositional environment [26–29].

The strata of the Wufeng Formation–Longmaxi Formation in the study area are fully developed, and no units are missing [17,18]. Among them, the strata of the Wufeng Formation are relatively thin (about 7 m; Figure 2), and they can be divided into three lithologic members from bottom to top. Lithologic member W1 is mainly composed of gray clay shale. Both lithologic members W2 and W3 are mainly composed of gray-black siliceous shale, and the top Guanyinqiao (GYQ) bed (generally less than 0.2 m thick), which is the boundary between the Wufeng Formation and the Longmaxi Formation, is mainly composed of deep-water siliceous shales and a small amount of calcareous biological debris [30] (Figure 4). The Longmaxi Formation can be divided into three lithologic members from bottom to top. Lithologic member L1 is composed of black-dark gray siliceous and gray clay shales, with bottom is rich in organic matter and total organic carbon (TOC) contents that are generally greater than 0.5%. Lithologic member L2 is composed of light gray-grayish green clay shale or

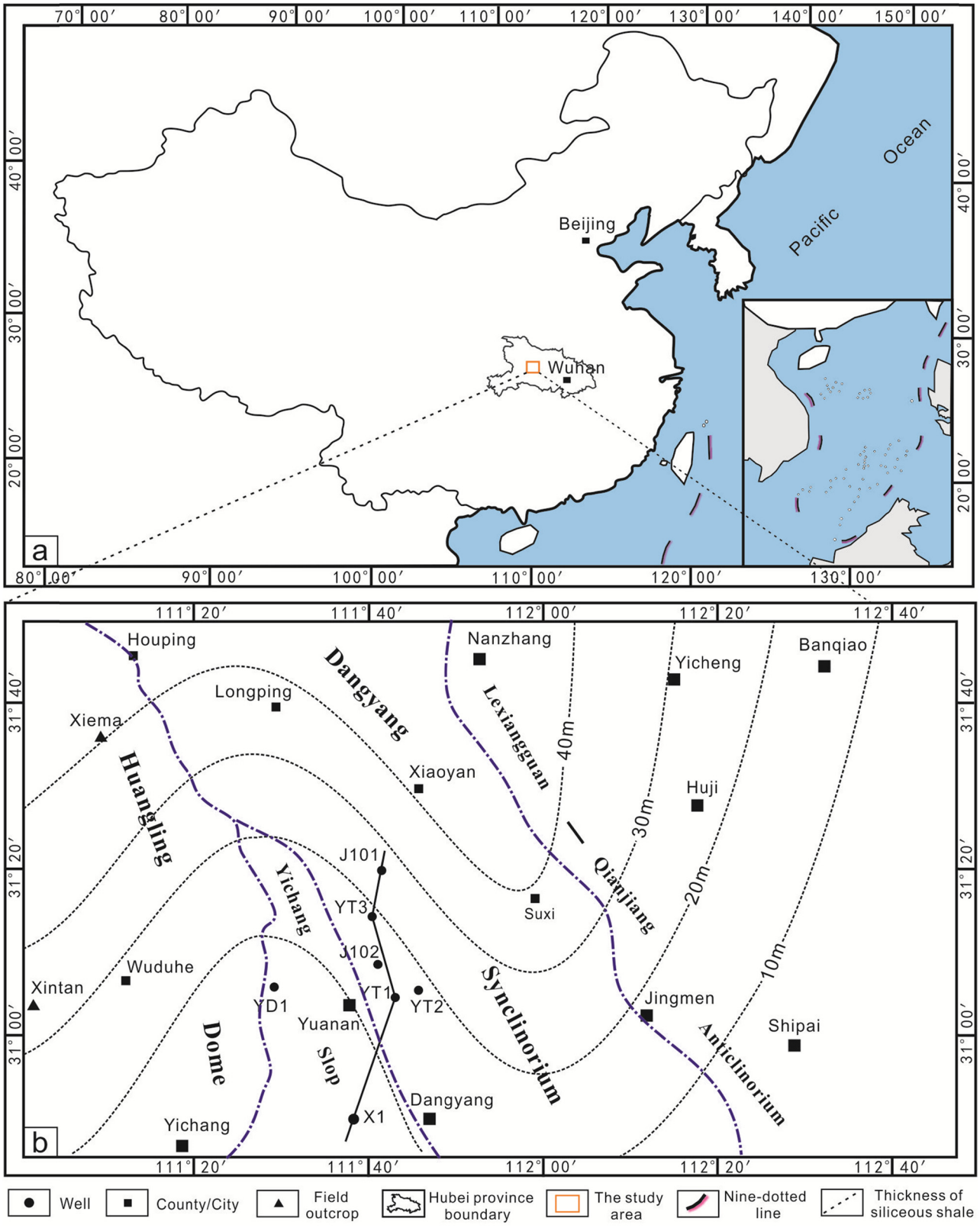

Figure 1: (a) Geographical location of the study area; (b) the regional distribution of the siliceous shale thickness (adapted from ref. [14]).

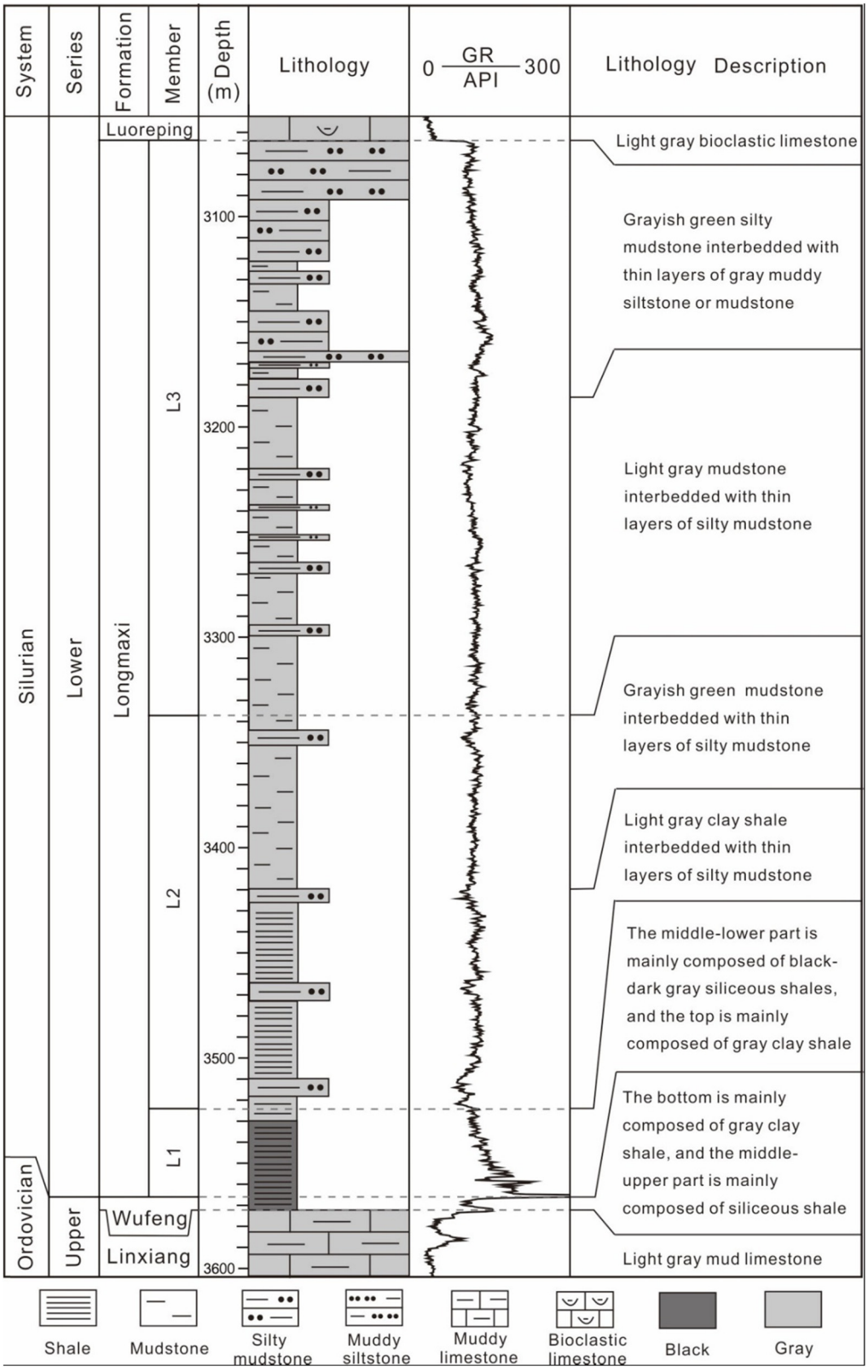

Figure 2: Stratigraphic column of the Wufeng Formation–Longmaxi Formation in well YT3. GR – natural gamma ray. API – American Petroleum Institute.

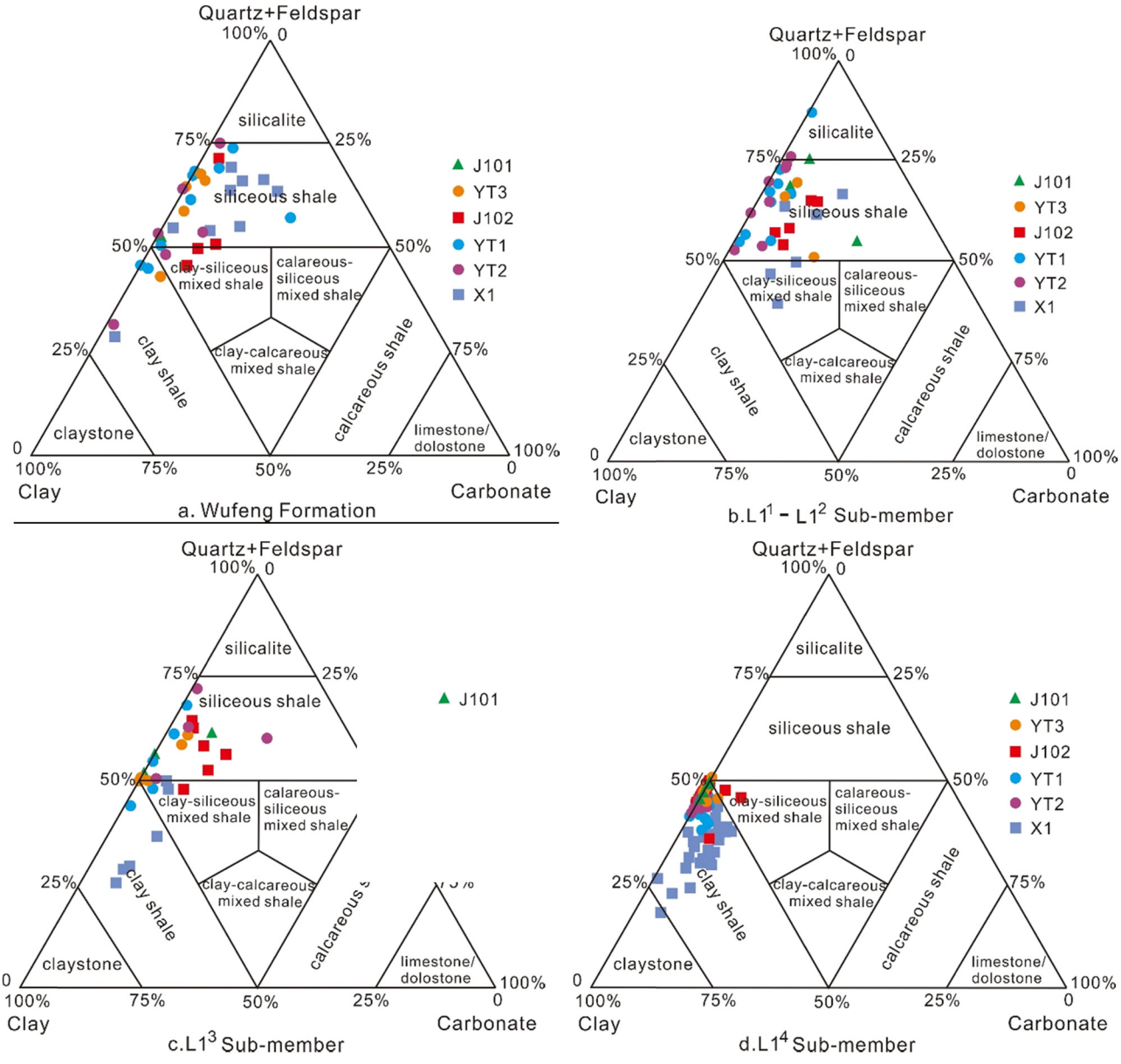

Figure 3: Ternary diagram for classifying the types of shale in the Wufeng Formation-Member L1 in the study area.

mudstone interbedded with thin layers of silty mudstone, with TOCs that are generally less than 0.5%. Lithologic member L3 is composed of grayish green-light gray silty mudstone or mudstone interbedded with thin layers of gray muddy siltstone, with TOCs that are generally less than or equal to 0.5% (Figure 2). This study focuses on the Wufeng Formation-Member 1 of the Longmaxi Formation (hereinafter referred to as L1 Member), which can be divided into four submembers from bottom to top (hereinafter referred to as $L1^1$, $L1^2$, $L1^3$, and $L1^4$) according to the morphological characteristics of the natural gamma ray (GR) curve (Figure 4). From the north to the south, the thickness of each submember decreases (Figure 8).

3 Sampling and analytical methods

The 257 specimens in this study were all collected from the black graptolite shales at the bottom of the Wufeng Formation–Longmaxi Formation in the shale gas exploration wells in western Hubei, of which 48 were from well YT1, 73 were from well YT2, 56 were from well YT3, 36 were from well J101, and 44 were from well J102. All of the specimens were identified through conventional thin section observations under a microscope to ensure the reliability of the specimen classification. Based on this, the specimens were selected for organic carbon analysis, X-diffraction analysis, focused ion beam-scanning electron

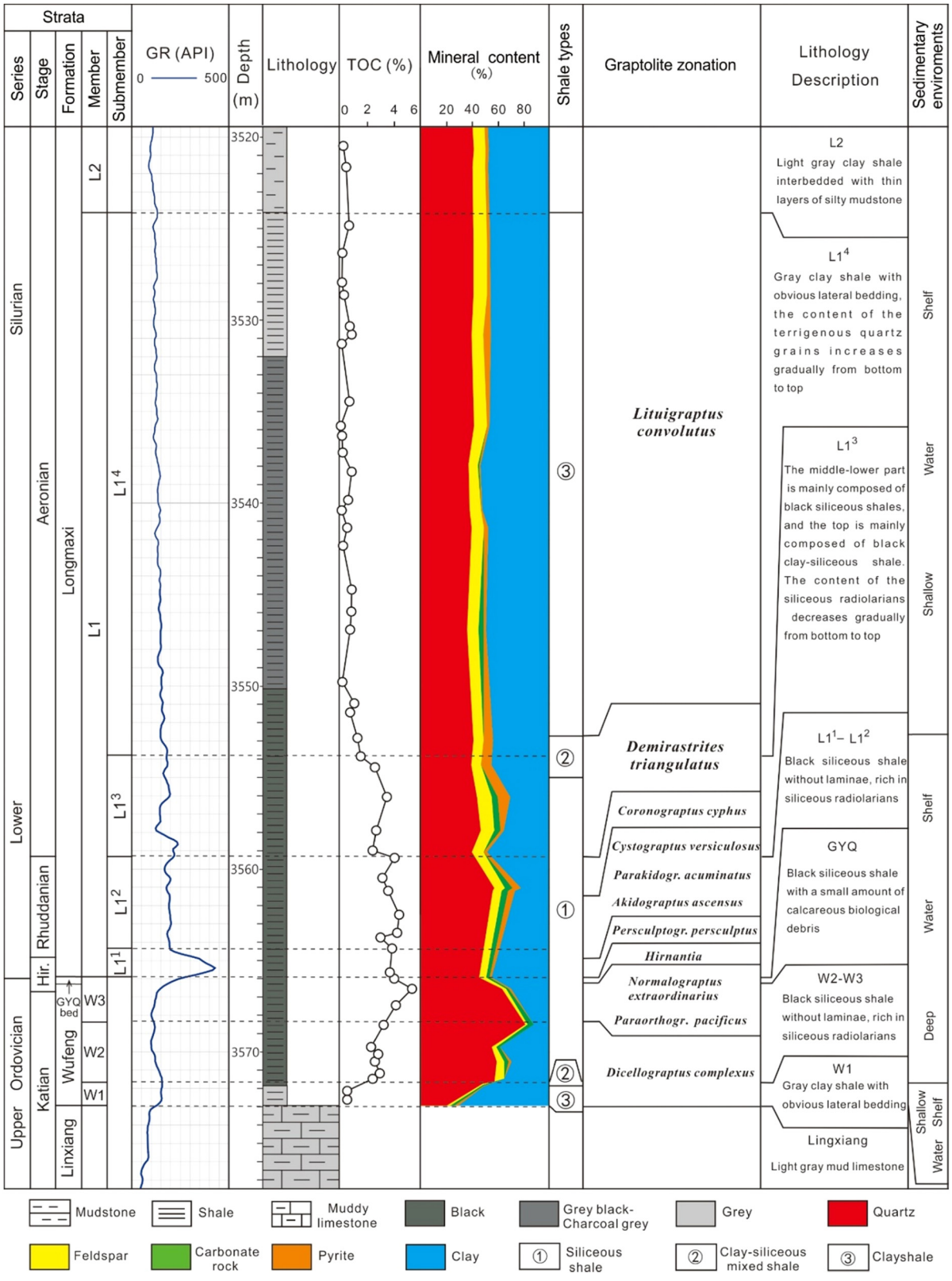

Figure 4: Comprehensive stratigraphic column of the Wufeng Formation-Member L1 in well YT3. GR – natural gamma ray. API – American Petroleum Institute. Hir. – Hirnantian. GYQ – Guanyinqiao, corresponding to Hirnantia. The graptolite zonation is from Chen et al. (2018b).

microscopy (FIB-SEM), and elemental analysis. In particular, the shale specimens selected for the FIB-SEM analysis were milled using an argon ion beam, and then, they were coated with a carbon film. The distribution of the sampling wells is shown in Figure 1b.

The analysis and testing of all of the shale specimens were performed in the geological laboratory of the Exploration and Development Research Institute of PetroChina Southwest Oil and Gas Field Company. The conventional thin section observations were performed using a LEICA DM2700P polarizing trinocular microscope. The TOC was measured using a CS-344 carbon-sulfur analyzer with a precision of ±0.5%. The X-ray diffraction measurements were conducted on a Phillips X'pert-MPD X-ray diffractometer, and the type and contents of the minerals were determined using the 2θ angle (scanning range of 20°–40°) and the diffraction peak intensity. The FE-SEM analysis was performed using a ZEISS Sigma-300 field emission-environmental SEM. The major elements analysis was performed on a Rigaku 100e wavelength-dispersive X-ray fluorescence spectrometer using fused glass discs prepared through the alkali fusion of the specimens. The trace and rare earth elements were analyzed using a Thermo Scientific Element XR Inductively coupled plasma mass spectrometer (ICP-MS).

4 Results and discussion

4.1 Shale classification scheme

Due to the improvement in data accessibility and characterization methodology, the shale classification schemes used in fine-grained sedimentology are becoming more diverse. Color, mineral composition, grain size, and lamination features were used as the classification parameters in the early schemes [31–33]. As research progressed, researchers now often include the main mineral contents, paleontological features, and organic matter enrichment, as well as the features of special minerals (such as nodules and pyrite) as shale classification parameters [4,6,34]. However, a unified classification standard for shales is still lacking. A reasonable shale classification scheme should not only focus on the shale petrology, depositional environment (i.e., the genesis), and other key factors, but it should also reflect the main mineral types of the shale formations. As for special formations such as those of nodules, pyrite bands, shell layers, and bentonite, they are usually not more than 0.5 m in thickness and have a limited distribution, so they can be ignored [34].

Given the above context, in this study, the shale classification was performed using a siliceous mineral (quartz + feldspar)-carbonatite mineral-clay mineral ternary diagram. That is, the shales were first classified as siliceous shales (siliceous content of greater than 50%), calcareous shales (calcareous content of greater than 50%), clay shales (clay content of greater than 50%), and mixed shales (siliceous, calcareous, and clay contents of greater than 25% but less than 50%) according to the criteria for the classification of sedimentary rocks. The above four types of shales were further subdivided into nine types according to the threshold proportions (25, 50, and 75%) of the three components in the ternary diagram (Figure 3). The introduction of lamination features, paleontological features, and groundmass fabrics as supplementary factors in the classification would lead to the use of numerous and complex terms for the shale types, which is of little research significance in practical applications, so these three supplementary factors were not considered in this study. Instead, key relevant factors were analyzed when comparing the development features of the different shale types.

4.2 Development and distribution characteristics of the different shale types

As can be seen from the ternary diagram and the whole-rock XRD results, the Wufeng Formation-Member L1 in the study area is mainly composed of siliceous shale, mixed clay-siliceous shale, and clay shale, with no samples plotting in the fields of calcareous-siliceous shale, clay-calcareous shale, or calcareous shale (Figure 3). The three main components above will be elaborated upon in terms of their colors, sedimentary structures, paleontological features, groundmass fabrics, and organic matter enrichments to reveal their basic characteristics and genesis.

4.2.1 Siliceous shales

Black siliceous shales were developed inside the strata from the W2 member to the $L1^3$ submember, corresponding to a total of nine graptolite zones of *D. complexus*–*D. triangulatus* (Figures 3a–c and 4). This is the main rock type in the study area, and it exhibits vertical depositional continuity, with the GYQ bed (siliceous shales) failing to separate the upper and lower layers (Figure 5a). The black siliceous shales do not contain laminae (Figure 5b), but they do contain rhabdosomes with high abundances and diversity, which are well preserved and disorderly arranged

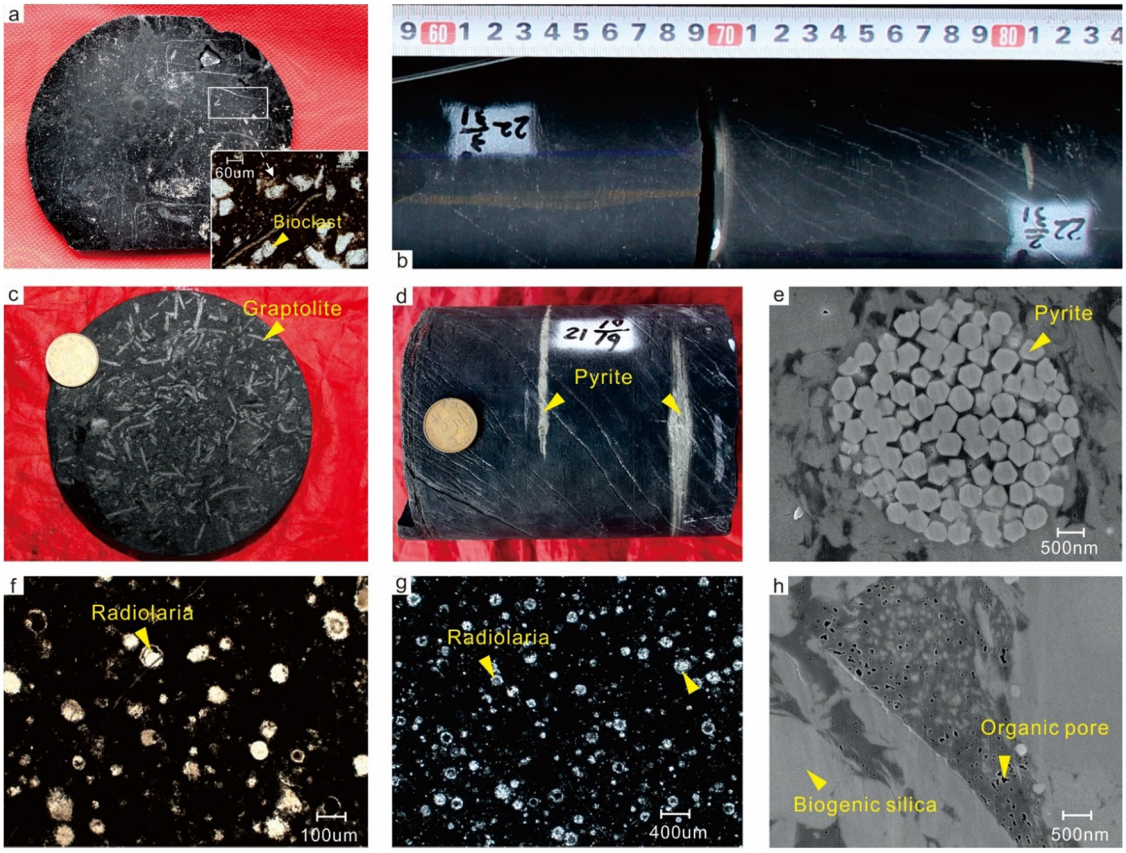

Figure 5: Depositional features of the siliceous shale. ((a) Black siliceous shale mixed with calcareous biological debris, at 3635.97 m in well YT3 in the GYQ bed; (b) absence of laminae, at 3561.7–3561.9 m in well YT3 in the $L1^2$ submember; (c) abundant graptolites with a disorderly arrangement, at 3978.14 m in well YT2 in the $L1^2$ submember; (d) strips of pyrite distributed in the siliceous shale, at 3559.5 m in well YT3 in the $L1^2$ submember; (e) SEM image showing abundant strawberry-shaped pyrite nodules in the siliceous shale, at 3978.7 m in well YT2 in the $L1^2$ submember; (f) thin section photograph showing abundant radiolarians filled with siliceous minerals, at 3567.4 m in well YT3 in the W3 member, cross-polarized light (+); (g) thin section photograph showing abundant siliceous radiolarians, at 3563.5 m in well YT3 in the $L1^2$ submember, cross-polarized light (+); (h) organic matter dispersed among biogenic siliceous grains forming a large number of organic pores, at 3974.3 m in well YT2 in the $L1^3$ submember. The coins in the images are 20.5 mm in diameter).

(Figure 5c). Pyrite was developed in large quantities and is often present as strips (with thicknesses of 1–2 cm; Figure 5d) or strawberry-shaped nodules (Figure 5e). Framework grains are common, mainly including radiolarians and some sponge spicules, which are generally filled by siliceous minerals (Figure 5f and g). The black siliceous shales are rich in siliceous minerals (quartz + feldspar), with a mean content of 60.6%, and are dominated by quartz (mean content of 54.6%; Figures 3 and 4). The quartz grains are mostly microcrystalline and powder crystalline grains of biological origin in a circular-subcircular shape [14,16], accompanied by minor amounts of subangular terrigenous quartz grains [9]. The carbonatite content is low (mean of 6.3%), occurring as calcite and dolomite cement. The clay mineral content is low, with a mean of 28.3%. The overall TOC content of the black siliceous shales is the highest of all the shale types, with an average of 3.95%. The TOC contents of the different strata decrease in the order of GYQ bed (4.15%) > $L1^1$–$L1^3$ submembers (mean of 3.51%) > W2 member (mean of 2.89%; Figure 4). The organic matter is dispersed between the clay minerals and the biogenic siliceous grains, and the black shale contains a large number of organic pores (Figure 5h).

The black siliceous shales are rich in pyrite, biogenic silica, and organic matter, but they lack laminae, indicating that the shales were deposited on a deep-water shelf where the hydrodynamic conditions were weak and the water was highly reducing (Figure 4).

4.2.2 Clay-siliceous mixed shales

The grayish black mixed clay-siliceous shales are mainly developed in the W1 member and at the junction of the

$L1^3$ and $L1^4$ submembers, corresponding to the *D. complexus* and *D. triangulatus* graptolite zones, respectively (Figures 3a, c, d, and 4). The mixed clay-siliceous shales differ from the siliceous shales mainly in the following aspects. (1) The hand specimens of the mixed clay-siliceous shales exhibit continuous, lateral sandy laminae that are generally no more than 5 mm thick (Figure 6a), and horizontal continuous laminae were also observed under the microscope (Figure 6b). (2) The scale of the pyrite is smaller in the mixed clay-siliceous shales. The pyrite bands are generally less than 5 mm thick (Figure 6c). (3) The mixed clay-siliceous shales are rich in clay minerals (mean content of 44.5%) but are poor in quartz (mean content of 38.2%), and the quartz grains are mainly subangular-subcircular microcrystalline grains with a few fine-powder crystalline grains. The abundance of siliceous radiolarians is significantly lower, and the quartz grains are often clustered, forming a band-shaped pattern mixed in an clay groundmass rich in organic matter (Figure 6b). (4) The organic matter content drops to a mean of 2.67%, and accordingly, the development of the organic pores is also lower (Figure 6d).

The mixed clay-siliceous shales are a transition type between the siliceous shales and the clay shales. Although they have been affected by the terrigenous clastic supply to some extent, their depositional characteristics still reflect that they were formed in an anoxic, weak, hydrodynamic environment on a deep-water shelf, but the water they were deposited in was not as deep as the water the siliceous shales were deposited in.

4.2.3 Clay shales

The gray-dark gray clay shales are mainly developed in the W1 member and $L1^4$ submember corresponding to the *D. complexush* and *L. convolutus* graptolite zones, respectively (Figures 3a, d, and 4), and they constitute the main lithofacies developed in the study area. The hand specimens show a large number of 1–3 cm thick, light gray, silty shale bands, indicating obvious lateral bedding (Figure 7a and b). The microscopic observations also reveal the lateral lamination of silty quartz clasts (Figure 7h). The scale of the pyrite is the smallest of all the shale types, generally occurring in a lenticular form or as clumps with poor stratification (Figure 7c). Graptolites occur with low abundance and diversity, are dominated by *C. cyphus* and *D. triangulatus*, and exhibit obvious directional alignment (Figure 7d). Furthermore, the clay shales contain a small amount of brachiopods (Figure 7e), Cyrtoceras (Figure 7f), and fossil tubes (Figure 7g), as well as other fossils and remains of benthic organisms. The quartz content is the lowest of all the shale types, with an average of 35.5%. The quartz grains are mainly subangular fine-powder crystals and mainly originated from a terrigenous supply. They generally occur as bands (Figure 7h) and dispersed grains

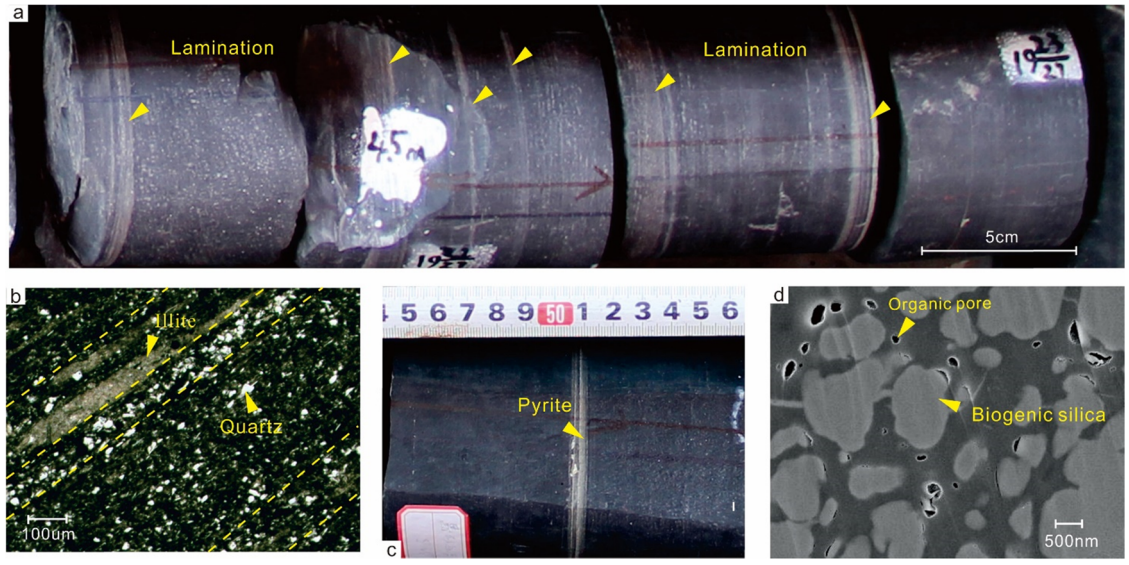

Figure 6: Depositional features of the mixed clay-siliceous shale. ((a) Lateral sandy laminae, at 3553.44–3553.69 m in well YT3 in the $L1^3$ and $L1^4$ submembers; (b) thin section photograph showing the uneven distribution of quartz, feldspar, mica, and illite, mostly clustered in strips, forming obvious lateral laminae (yellow deficiency line), at 3554.4 m in well YT3 in the $L1^3$ submember, plane-polarized light (–); (c) pyrite distributed in a strip, at 3554.69 m in well YT3 in the $L1^3$ submember; (d) SEM image showing that the development of the organic pores is lower than that of the siliceous shale, at 3970.3 m in well YT2 in the $L1^3$ submember).

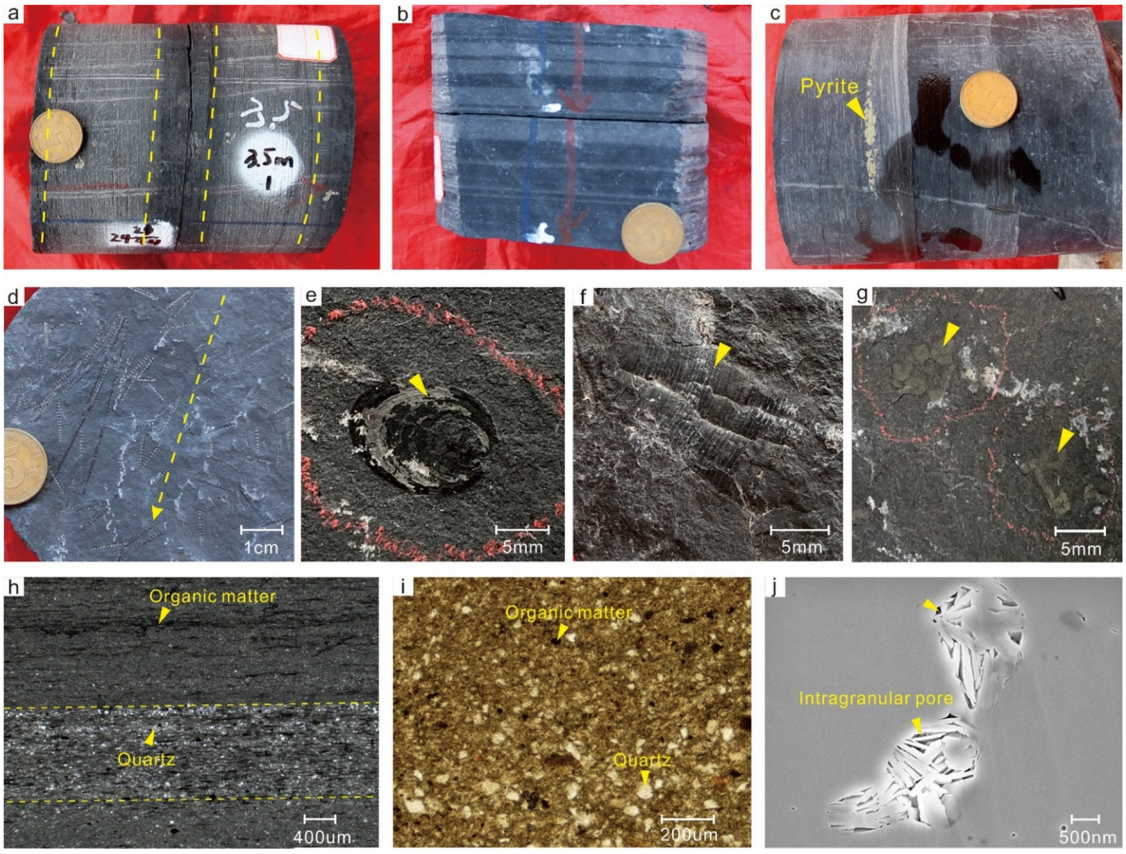

Figure 7: Depositional characteristics of the clay shale. ((a) Lateral bedding, at 3572.6 m in well YT3 in the W1 member; (b) light gray silty shale bands with lateral bedding, at 3531.2 m in well YT3 in the $L1^4$ submember; (c) lenticular pyrite with poor stratification, at 3538.7 m in well YT3 in the $L1^4$ submember; (d) graptolites with a low abundance and diversity exhibiting an obvious directional arrangement, at 3537.4 m in well YT3 in the $L1^4$ submember. The yellow arrow indicates the arrangement direction of the graptolites; (e) brachiopod fossils, at 3572.7 m in well YT3 in the W1 submember; (f) cyrtoceras, at 3526.4 m in well YT3 in a single layer of the $L1^4$ submember; (g) fossil tube, at 3536.1 m in well YT3 in the $L1^4$ submember; (h) thin section photograph showing the presence of clay-rich laminae sandwiching quartz clast-rich laminae and the presence of a low content of organic matter distributed intermittently in the form of fine laminae, at 3531.29 m in well YT3 in the $L1^4$ submember, cross-polarized light (+); (i) thin section photograph showing fine-powder quartz grains dispersed in a clay-rich groundmass with a small amount of organic debris, at 3,468 m in well YT1 in the $L1^4$ submember, plane-polarized light (–); (j) SEM image showing intergranular pores between clay minerals with few organic pores, at 3964.2 m in well YT2 in the $L1^4$ submember. The coins in the images are 20.5 mm in diameter).

(Figure 7i) in a clay-rich groundmass. Subcircular siliceous radiolarian grains of biological origin are extremely rare. The carbonatite content is low, with a mean of 3%, and mainly occurs in the form of crack-filling calcite. The clay mineral content is the highest of all the shale types, with an average of 54.3%. The organic matter content is the lowest of all the shale types, with a mean of only 0.44%. The microscopic observations reveal that the organic matter is usually scattered in the clay mineral groundmass in the form of discrete, fine-grained, laminae, or clasts (Figure 7h–i), and organic pores are rare, in contrast to the large amount of inorganic pores (Figure 7j). The above features indicate that the clay shales were formed in a shallow-water, oxygen-rich, strong hydrodynamic environment on a shallow-water shelf.

4.2.4 Spatial distribution characteristics of the different shale types

4.2.4.1 Vertical evolution characteristics

The Wufeng Formation–Longmaxi Formation in the Yangtze region is a graptolite shale formation formed by the alternating glacial and interglacial periods during the Ordovician-Silurian transition [35]. The shales are characterized by multiple depositional cycles in the vertical direction, with strong heterogeneity and a generally tripartite character (Figure 4). During the depositional period of the W1 member, the study area was in the initial stage of the platform-to-shelf transition with shallow depositional water depths, that is, it was in a

shallow-water shelf depositional environment. During this period, the rocks were dominated by clay shale deposits, and internal laminae developed. As the water depth increased, the shales transitioned to mixed clay-siliceous shales, which were deposits at the end of the depositional period of the W1 member (Figure 4). During the depositional period of W2–$L1^3$, the study area was in a continuous, deep-water shelf depositional environment, in which the rocks were dominated by siliceous shales, and internal laminae did not develop (Figure 4). From the late depositional period of the $L1^3$ submember to the depositional period of the $L1^4$ submember, the depositional water depths continued to decrease, and accordingly, the depositional environment transitioned from a deep-water shelf environment to a shallow-water shelf environment, with the rocks rapidly transitioning from mixed clay-siliceous shales to clay shales (Figure 4) and forming a large number of lateral beds.

4.2.4.2 Lateral distribution characteristics

The shales of the Wufeng Formation-Member L1 in western Hubei have a distinct tripartite character in the north–south direction, but there are differences among the different shale types in terms of their development layers and depositional thicknesses. The early-middle stage of the W1 member is mainly composed of clay shales, while it is dominated by mixed clay-siliceous shales in the late stage. The two types of shales are distributed stably in the lateral direction without significant changes. During the depositional period of W2–$L1^3$, the shale types in well X1 in the southern part of the study area changed from siliceous shale, to mixed clay-siliceous shale to clay shale from bottom to top, with the siliceous shales ending their development in the early depositional period of $L1^2$. Extending northward from well X1 to well YT1 and further to well YT3, the shale facies show a vertical transition trend from siliceous shale to mixed clay-siliceous shales, with the siliceous shales ending their development in the late depositional period of $L1^3$ with a significant increase in thickness. Farther north, in well J101, the formation is dominated by siliceous shale and it becomes thicker. During the depositional period of $L1^4$, the study area was mainly dominated by clay shale deposits, and there was no significant change in the shale's thickness. The siliceous

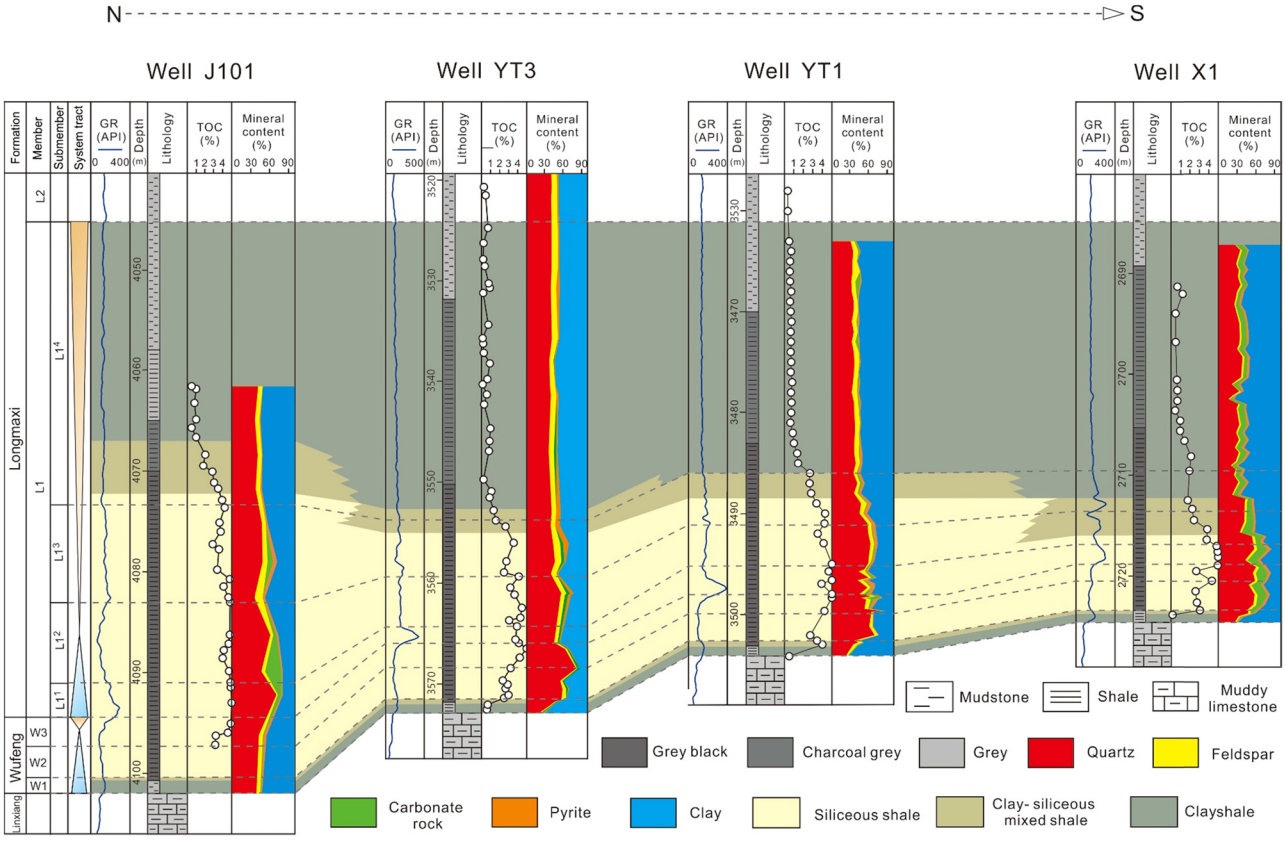

Figure 8: Shale type comparison among wells J101, YT3, YT1, and X1 in the Wufeng Formation-Member L1 in western Hubei. GR – natural gamma ray. API – American Petroleum Institute.

shales and mixed clay-siliceous shales mainly occurred in the early depositional period of $L1^4$ in well J101 in the northern part of the study area (Figure 8).

As shown above, the siliceous shales in the study area gradually thicken, and their development ended at an increasingly late time to the north (Figure 8). Moreover, the siliceous shales significantly thicken to the north and northwest (Figure 1b). These changes occurred in response to the Caledonian movement on the Yangtze Platform. During the Caledonian period, as the Cathaysian Oldland continued to collide with the Yangtze Platform from southeast to northwest, the depocenter of the shales migrated northwestward, which resulted in the abovementioned changes in the rock type in the study area.

4.3 Depositional environments of the different shale types

4.3.1 Ancient sea-level changes

Previous studies have shown that it is possible to infer ancient sea-level changes from Ce anomalies [36,37]. The shales of the Wufeng Formation-Member L1 in the study area exhibit obvious negative Ce anomalies (Figure 9 and Table 1). The early-mid depositional period of W1–W3 corresponds to the first large-scale marine transgression during the Ordovician-Silurian transition when the sea level gradually rose due to a global marine transgression [14,38], producing mainly negative Ce anomalies. At the end of the depositional period of W3 (the Hirnantian Ice Age), the climate became colder, with the seawater beginning to solidify and the global sea level beginning to fall, which led to a significant δCe shift toward smaller negative Ce anomalies, with δCe reaching its lowest value (0.61) in the entire member at GYQ. In the depositional period of $L1^1$, the global climate warmed, with the ice sheet melting and the sea level rapidly rising, which caused the δCe to rapidly increase, followed by a continuous rise in sea level until the highest sea level occurred in the middle of the depositional period of $L1^2$, corresponding to the second large-scale marine transgression during the Ordovician-Silurian transition. Thereafter, as the downward flexure in the southeastern part of the Yangtze Platform increased, the depocenter began to migrate northwestward [35], while the sea level began to fall. Despite several fluctuations in δCe, it generally shifted toward smaller negative Ce anomalies (Figure 9 and Table 1).

As shown above, the clay shales were formed in a relatively low water-level period, mainly in the early stage of the sea-level rise and in the late stage of the sea-level drop; while the siliceous shales were formed in a relatively high sea level period, mainly in the mid-late stage of the sea-level rise and in the early stage of the sea-level drop. The mixed clay-siliceous shales are a transitional type between the two, which formed in an intermediate water-level period (Figure 9). It is noteworthy that although a global sea-level drop took place in the late stage of W3 (the Hirnantian Ice Age), the main part of the study area was in a depression far away from the underwater paleo-uplifts, and therefore, it still had a relatively high water level [14,30]. This area is mainly composed of siliceous shales.

4.3.2 Paleoredox conditions

Trace element indicators of redox conditions such as the Ni/Co and V/Cr ratios are widely used to assess ancient redox conditions [39]. As shown in Figure 9 and Table 1, the vertical changes in the Ni/Co and V/Cr ratios were relatively consistent. During the depositional period of W1, the rocks were mainly clay shales, and both their Ni/Co and V/Cr ratios indicate an oxygen-rich water environment. During the depositional period of W2–$L1^3$, the rocks were dominated by siliceous shales, and their Ni/Co and V/Cr ratios are indicative of an anoxic-suboxic environment. During the interval from the late depositional period of $L1^3$ to the early depositional period of $L1^4$, the rocks were mainly mixed clay-siliceous shales with intermediate Ni/Co and V/Cr ratios, indicating that the shales were deposited in a transitional depositional environment between a suboxic depositional environment and an oxygen-rich depositional environment, but the environment was generally closer to the former. Thereafter, the rocks were mainly composed of clay shales with low Ni/Co and V/Cr ratios, which are indicative of a stable, oxygen-rich water environment.

As indicated by the redox indicators discussed above, the siliceous shales were generally formed in an anoxic-suboxic water environment; the mixed clay-siliceous shales were mainly formed in an anoxic water environment and thus had a lower reducibility than the siliceous shales; and the clay shales were formed in a relatively stable, anerobic water environment. In addition, the TOC exhibits a clear linear relationship with the Ni/Co and V/Cr ratios. With the gradual weakening and disappearing of the anerobic environment in the order of siliceous shales, mixed clay-siliceous shales, and clay shales, the preservation conditions of the organic matter were affected, leading to a gradual decrease in the TOC values (Figure 9 and Table 1).

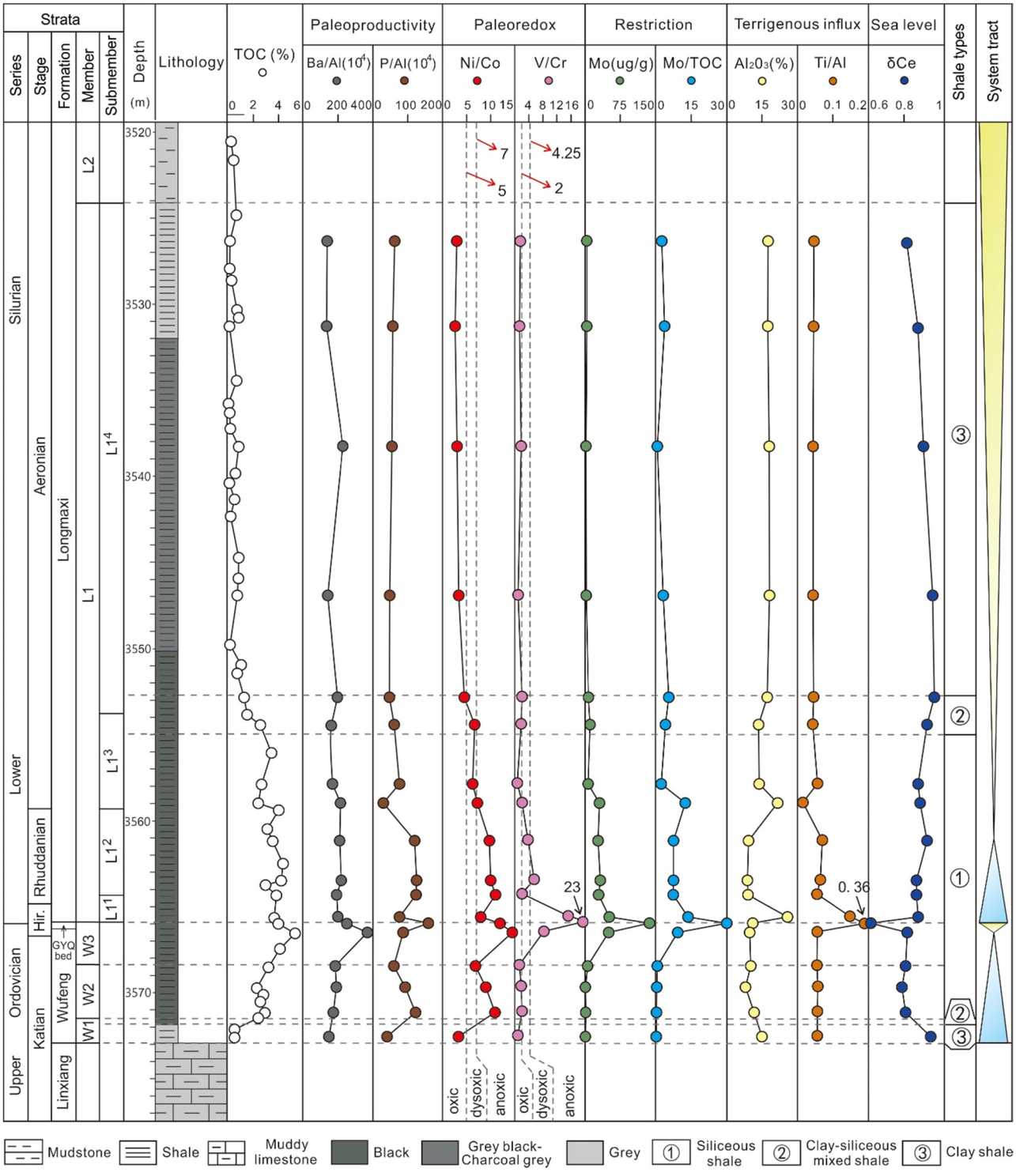

Figure 9: Vertical distribution of the geochemical parameters of the different rock types in well YT3 in the Wufeng Formation-L1 Member. Hir. – Hirnantian. GYQ – Guanyinqiao. For the redox discrimination parameters refer to [39].

4.3.3 Terrigenous input

Al and Ti are the main elements in the continental crust, so the Al_2O_3 content and Ti/Al ratio are often used to assess the terrigenous input to ancient and modern oceans [24,40,41]. The clay shales in W1 (early stage of sea-level rise) and $L1^4$ (mid-late stage of sea-level drop) were formed in shallow depositional water bodies with high terrigenous

Table 1: Composition and calculation results of the major, trace, and rare earth element concentrations of the different shale types in well YT3 in the Wufeng Formation-Member L1 in western Hubei

Sample no.	YT3-13-7	YT3-15-1	YT3-17-2	YT3-18-2	YT3-19-9	YT3-19-15	YT3-21-1	YT3-21-3	YT3-21-7	YT3-22-5	YT3-22-7	YT3-22-9	YT3-GYQ-1	YT3-22-11	YT3-23-3	YT3-24-2	YT3-24-5	YT3-24-8
Stage	Aeronian								Rhuddanian			Hirnantian			Katian			
Horizon	$L1^4$	$L1^4$	$L1^4$	$L1^4$	$L1^4$	$L1^3$	$L1^3$	$L1^3$	$L1^2$	$L1^2$	$L1^1$	$L1^1$	GYQ bed	W3	W2	W2	W2	W1
Rock types	③	③	③	③	②	②	①	①	①	①	①	①	①	①	①	①	①	③
Depth/m	3526.33	3531.29	3538.28	3546.93	3552.84	3554.44	3557.89	3558.99	3561.19	3563.49	3564.34	3565.64	3565.99	3566.54	3568.49	3569.72	3571.17	3572.6-0
TOC/%	0.26	0.20	0.94	0.84	1.30	2.67	2.78	2.51	3.67	4.33	3.95	3.79	4.15	5.44	3.26	2.38	3.03	0.60
Al_2O_3/%	17.64	17.47	18.04	18.15	17.23	13.63	13.80	21.65	9.30	8.78	9.11	25.84	11.11	9.73	10.26	8.02	11.63	14.99
Ba/(μg/g)	1292.18	1256.40	2194.79	1365.90	1806.65	1175.98	1227.31	2462.22	1037.01	1021.11	933.27	2754.32	1470.00	1908.38	1003.75	814.14	1069.87	1172.83
P/(μg/g)	0.06	0.05	0.05	0.05	0.04	0.04	0.06	0.04	0.06	0.06	0.06	0.11	0.09	0.04	0.03	0.04	0.08	0.03
Ti/(μg/g)	0.44	0.43	0.43	0.43	0.42	0.32	0.42	0.18	0.35	0.30	0.27	2.03	2.09	0.29	0.30	0.25	0.35	0.45
Al($\times10^{-4}$)/(μg/g)	9.33	9.25	9.55	9.60	9.12	7.22	7.30	11.46	4.92	4.64	4.82	13.68	5.88	5.15	5.43	4.24	6.15	7.93
Mo/(μg/g)	0.69	0.76	0.69	2.74	7.25	11.07	6.71	31.40	28.01	33.02	29.52	51.77	137.00	50.82	2.47	1.17	1.43	0.67
Ni/(μg/g)	55.03	45.12	50.67	64.62	82.13	100.22	69.12	82.36	129.19	141.79	172.44	163.91	219.54	184.66	40.03	45.70	86.24	101.17
Co/(μg/g)	18.37	17.00	16.60	18.94	17.98	14.98	10.95	11.33	13.21	14.02	15.61	20.53	18.38	12.66	5.83	5.05	7.88	30.10
V/(μg/g)	150.77	154.14	165.48	173.26	202.56	136.28	114.22	87.88	263.67	290.12	268.06	705.83	2688.49	1156.81	210.91	237.40	361.66	146.99
La/(μg/g)	61.18	54.30	59.51	53.32	54.22	49.74	40.31	41.08	35.53	36.12	33.18	176.62	34.59	34.43	45.53	31.21	42.87	53.96
Ce/(μg/g)	100.45	94.08	105.90	104.24	108.50	95.19	70.35	68.23	67.64	64.70	59.03	329.31	46.16	55.17	72.65	48.11	72.48	101.50
Pr/(μg/g)	12.78	10.90	11.63	11.84	12.39	11.50	8.27	6.88	8.09	8.13	7.32	43.34	9.24	6.65	9.24	6.20	10.02	10.93
Ba/Al($\times10^4$)	138.42	135.86	229.88	142.21	198.16	162.96	168.05	214.83	210.78	219.85	193.55	201.39	249.93	370.57	184.81	191.89	173.82	147.88
P/Al($\times10^4$)	63.37	57.91	55.53	49.09	48.49	61.92	77.03	31.05	120.73	126.31	124.40	77.16	159.81	87.23	61.46	93.35	122.89	41.70
Ni/Co	3.00	2.65	3.05	3.41	4.57	6.69	6.31	7.27	9.78	10.11	11.05	7.98	11.95	14.59	6.87	9.04	10.95	3.36
V/Cr	1.61	1.37	1.82	0.99	2.13	1.82	0.79	2.08	3.76	5.48	2.11	15.12	22.77	8.28	1.42	1.89	2.12	0.88
Mo/TOC	2.64	3.80	0.74	3.26	5.58	4.14	2.41	12.51	7.63	7.63	7.47	13.66	33.01	9.34	0.76	0.49	0.47	0.27
Ti/Al	0.0475	0.0462	0.0447	0.0447	0.0464	0.0442	0.0570	0.0160	0.0706	0.0654	0.0558	0.1488	0.3558	0.0562	0.0555	0.0582	0.0573	0.0567
δCe	0.82	0.88	0.91	0.96	0.97	0.93	0.88	0.89	0.93	0.87	0.87	0.88	0.61	0.82	0.81	0.79	0.81	0.95

Note: ① siliceous shale, ② mixed clay-siliceous shale, ③ clay shale. $\delta Ce = 2Ce_n/(La_n + Pr_n)$, where the subscript n denotes normalization to a standard mean value for the shales.

inputs, which resulted in high Al_2O_3 contents and low Ti/Al ratios. In contrast, the siliceous shale deposited in the W2–L1[3] depositional period was formed in a continuously deep water environment with low terrestrial inputs, which resulted in low Al_2O_3 contents and high Ti/Al ratios. The mixed clay-siliceous shales deposited from the late depositional period of L1[3] to the early depositional period of L1[4,] have Al_2O_3 contents and Ti/Al ratios between those of the clay shales and siliceous shales, indicating a moderate terrigenous input (Figure 9 and Table 1).

Terrigenous clastic inputs have multiple effects on shale composition. (1) Terrigenous clastic inputs dilute the organic matter and reduce its content [42]. That is, as the terrigenous input gradually increased in the order of siliceous shales, mixed clay-siliceous shales, and clay shales, the TOC gradually decreased, exhibiting an obvious dilution effect (Figures 8 and 9 and Table 1). (2) Terrigenous inputs change the mineral compositions and structures of shales. That is, due to the low terrigenous inputs, the siliceous shales have low clay mineral contents and did not form internal laminae, forming a blocky structure instead. The quartz was mainly biogenic and originated from siliceous radiolarians. As the terrigenous input increased, the clay mineral content increased, which was accompanied by a gradual increase in the content and grain size of the terrigenous quartz grains, leading to the gradual development of sandy laminae (Figures 5–7).

4.3.4 Degree of water restriction

The ratio of the redox-sensitive element Mo to the TOC is often used to determine the degree of seawater restriction. As shown in Figure 10, the lower the Mo/TOC ratio, the stronger the water restriction [43]. However, this hydrological analysis method is only applicable to anoxic facies subject to hydrographic restriction [43,44]. During the depositional periods of W1 and L1[4] when the clay shales were deposited in the study area, the water body was rich in oxygen with low Mo/TOC ratios, and the enrichment of Mo was mainly controlled by the redox conditions. This suggests that the Mo enrichment cannot be used to judge the degree of water restriction (Figure 10 and Table 1). During the depositional period of W2–L1[3] when the siliceous shales was deposited, the water body was anoxic-suboxic, and the Mo/TOC ratios exhibited an obviously bipartite character. (1) The Mo/TOC ratios of the three samples from W2 were far lower than the mean of 4.5 for the Black Sea and were close to the mean of 2.0 for the Barnett shales in the Fort Worth Basin where a high degree of water restriction occurred [45]. (2) The Mo/TOC ratios of the samples from W3–L1[3] indicate a semi-restricted marine basin. In particular, the GYQ bed exhibits the highest Mo/TOC ratio, which is close to those of the Cariaco Basin (mean of 25), suggesting that the GYQ was subject to the lowest degree of water restriction. In the interval from the late depositional period of L1[3] to the early depositional period of L1[3] when the mixed clay-siliceous shales were deposited, the water body was suboxic with Mo/TOC ratios close to those of the Black Sea, which indicate a strongly restricted marine basin. However, the degree of water restriction was lower than that of the W2 siliceous shales (Figures 9 and 10 and Table 1).

Tectonic movements and sea-level changes closely affect water restriction, and in turn, the exchange of

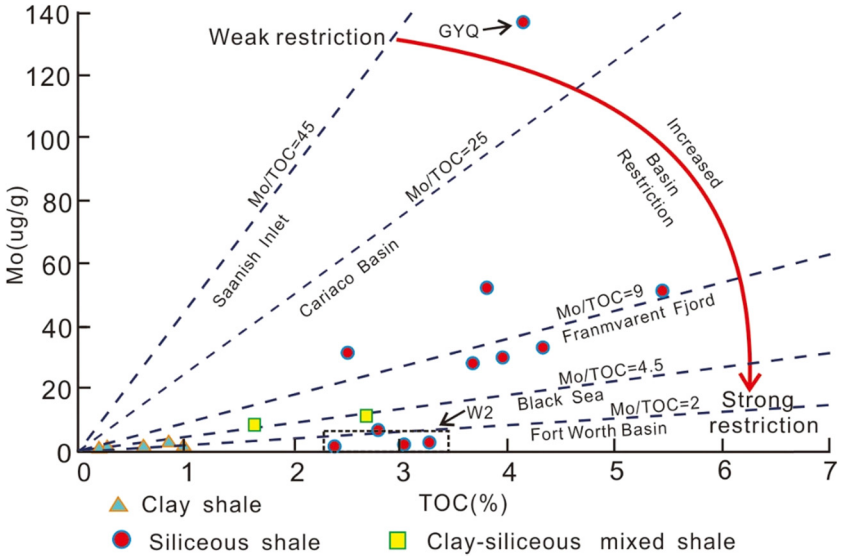

Figure 10: Comparison of the Mo/TOC relationships of the shales in well YT3 in the Wufeng Formation-Member L1 and shales formed in modern anoxic marine basins and the Fort Worth Basin. The Mo/TOC linear regression lines are from refs [44,45].

nutrients in the water bodies, which is of great significance to the accumulation of organic matter [24,41]. This study reveals that the TOC values of the W2 siliceous shales are lower (mean of 2.89%), which were formed in a strongly restricted environment, than those of the W3–$L1^3$ siliceous shales (mean of 3.83%), which were formed in a semi-restricted environment, but they are higher than those of the mixed clay-siliceous shales (mean of 2.15%), which were formed in a relatively weakly restricted environment (Table 1). Therefore, we propose that the restriction of the environment has a significant effect on the organic matter content of siliceous shales formed under high water levels, but has a relatively weak influence on mixed clay-siliceous shales formed under moderate water levels. In the latter scenario, the changes in the redox conditions and the terrigenous inputs due to sea-level changes are more critical to the organic matter enrichment.

4.3.5 Paleoproductivity

The Ba and P contents of marine sediments have been widely used as indicators of paleomarine productivity [46]. Since trace elements in sediments are generally derived from terrigenous clasts and authigenic materials, a common practice is to first normalize the Ba and P contents to the Al contents and to use the P/Al and Ba/Al ratios to represent the paleoproductivity corrected for the influence of terrigenous input [24,46]. During the depositional period of W1 and $L1^4$ when the clay shales were deposited, the Ba/Al and P/Al ratios were low, indicating a low paleoproductivity. During the interval from the late depositional period of $L1^3$ to the early depositional period of $L1^4$ when the mixed clay-siliceous shales were deposited, the Ba/Al and P/Al ratios were higher than those of the clay shales, indicating a higher paleoproductivity. During the depositional period of W2–$L1^3$ when the siliceous shales were deposited, the Ba/Al and P/Al ratios were the highest of all the shale types, indicating the highest paleoproductivity. Moreover, the changes in paleoproductivity exhibit a good correlation with the degree of water restriction during the development of the siliceous shales. That is, the W2 siliceous shales formed in a strongly restricted environment and had a significantly lower paleoproductivity, as indicated by the mean Ba/Al (183.51) and P/Al (92.57) ratios ($\times 10^4$), than the W3–$L1^3$ siliceous shales formed in a semi-restricted environment, with Ba/Al and P/Al ratios of 228.62 and 100.47, respectively. Furthermore, the GYQ bed, which is the top layer of W3, was formed in an environment with the weakest water restriction and had the highest paleoproductivity, as indicated by the highest mean P/Al (159.81) and Ba/Al (249.93) ratios ($\times 10^4$; Figure 10 and Table 1).

Changes in the initial productivity play a key role in the enrichment of organic matter [27,47–49]. In the study area, from the deposition of the siliceous shales to the mixed clay-siliceous shales to the clay shales, the paleoproductivity continued to decrease and the surface seawater nutrients gradually decreased, which led to a gradual decrease in the development scale of the plankton, such as radiolarians and graptolites (Figures 5–7), and thus a gradual decrease in the organic matter content. Moreover, the paleoproductivity during the deposition of the siliceous shales decreased in the order of the GYQ bed, the $L1^1$–$L1^3$ submembers, and the W2 member, which was accompanied by a similar trend in the TOC values (Figure 9 and Table 1).

4.4 Depositional evolution models for the different shale types

Based on the analysis of the development characteristics of the different rock types and their depositional environments conducted in this study, we propose that the paleoenvironmental evolution of the study area during the Late Ordovician-Early Silurian can be roughly divided into six main stages, with the clay shales mainly forming in stage A and stage F, the siliceous shales mainly forming in stages B, C, and D, and the mixed clay-siliceous shales mainly forming in stage E (Figure 11).

Stage A corresponds to the depositional period of the W1 member. Due to a global marine transgression [49], the study area rapidly transitioned from a platform to a shallow-water shelf [35]. The depositional water bodies were shallow and received high terrigenous inputs. The bottom water was mainly oxygen rich with benthic organism development, while the surface water was nutrient poor with a low paleoproductivity. As a result, a group of clay shales poor in organic matter and rich in terrigenous quartz clasts were deposited (Figure 11A).

Stages B, C, and D correspond to the depositional period of the W2 member (the preglacial period), the GYQ bed (the glacial period), and the $L1^2$ submember (the postglacial period), respectively. In particular, stage

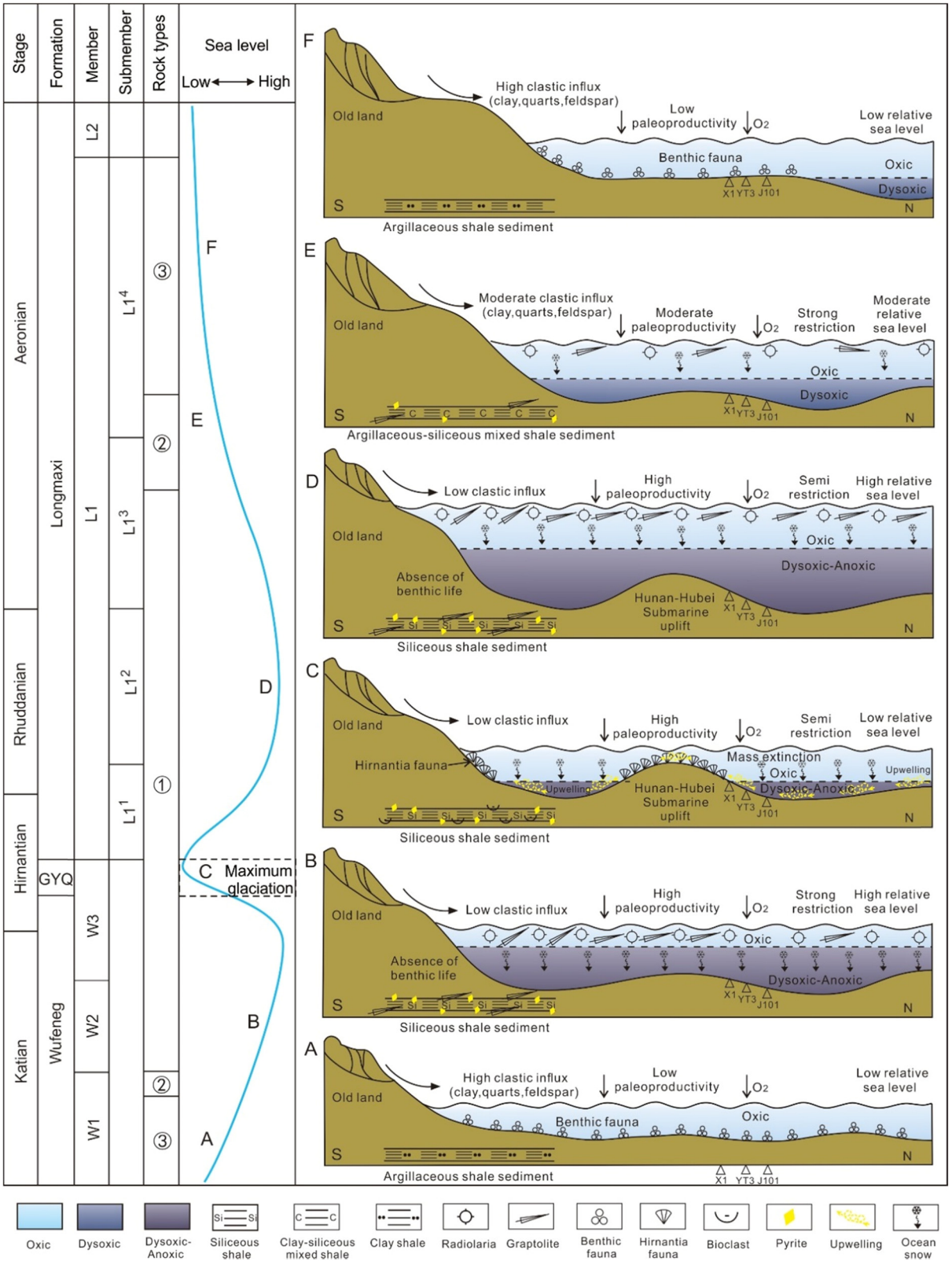

Figure 11: Formation and evolution model for the different rock types in the Wufeng Formation-Member L1 in western Hubei. GYQ – guanyinqiao, ① siliceous shale, ② mixed clay-siliceous shale, ③ clay shale.

B (Figure 11B) and stage D (Figure 11D) were both deposited in a period of continuous sea level rise, during which the bottom water was dominated by an anoxic-suboxic environment with low terrigenous inputs and the surface water was nutrient-rich and the paleoproductivity was high, which led to the development of siliceous shales rich in organic matter and biogenic silica. However, due to the continuous rise of the paleo-uplifts on the margin of the Yangtze Plate [35,38], the water restriction in stage B was stronger than in stage D, which weakened the nutrient exchange capacity with the open sea, resulting in a lower paleoproductivity and TOC in stage B than in stage D. Stage C corresponds to the strongest period of the Hirnantian Ice Age (Figure 11C), during which the climate became drastically colder, the sea level dropped significantly, and the chemical weathering weakened, resulting in low terrestrial inputs (Figure 9 and Table 1) [50]. In stage C, the range of the deep water shrank to the areas far away from the Hunan-Hubei submarine uplift [30] where the water environment was anoxic-suboxic and was dominated by siliceous shale deposits (containing calcareous bioclasts). The unusually active upwelling currents during the glacial period brought rich nutrients from the open sea (Figures 9 and 11C and Table 1) [49–53], resulting in a higher paleoproductivity than in the preglacial and postglacial periods and thus a higher organic matter content in stage C than in stages B and D.

Stage E corresponds to the interval from the late depositional period of submember $L1^3$ to the early depositional period of submember $L1^4$ (Figure 11E). Due to the Guangxi Movement, the collision and amalgamation between the Yangtze Plate and the adjacent blocks strengthened, leading to the further uplift of the uplifts on the margin of the Yangtze Plate, the subsidence and disappearance of the Hunan-Hubei submarine uplift, and shrinkage of the sea area and a rapid drop in sea level to a moderate range [24,35,38]. Compared with stage D, the water restriction was higher in stage E (i.e., formation of a strongly restricted marine basin), the oxygen-poor conditions were worse (i.e., predominantly suboxic), and the terrigenous inputs increased, leading to a decrease in the paleoproductivity and thus a decrease in the TOC.

Stage F corresponds to the middle to the late depositional period of submember $L1^4$, and the depositional environment was significantly different from that of stage A (Figure 11F). During this period, the collision between the Yangtze Pate and the adjacent blocks continued to strengthen and the surrounding paleo-uplifts continued to rise, which led to a dramatic drop in sea level. The area of present-day western Hubei was dominated by shallow waters, which were primarily oxygen-rich and hosted benthic organism development; while the deep-water sediments migrated to the Nanzhang area in the northern part of the study area [14,38]. The terrigenous inputs increased rapidly and the paleoproductivity continued to decrease, eventually leading to the formation of a group of clay shales poor in organic matter and rich in terrigenous quartz clasts.

In summary, the formation of the different rock types in the Wufeng Formation–Longmaxi Formation is the comprehensive result of the evolution of the Ordovician-Silurian depositional environment. The tectonic conditions, sea-level, paleoredox conditions, paleoproductivity, terrigenous inputs, and degree of water restriction jointly controlled the mineral compositions and structures and the organic matter enrichments of the different types of rocks.

5 Conclusion

(1) The marine shales of the Wufeng Formation-Member L1 in western Hubei were classified as siliceous shales, mixed clay-siliceous shales, and clay shales using a ternary diagram. Siliceous shales are a rock type unique to deep-water environments, clay shales are the main rock type deposited in shallow-water environments, and mixed clay-siliceous shales are in between. In the order of siliceous shales, mixed clay-siliceous shales, and clay shales, the content of biogenic silica, the development of pyrite, the abundance of graptolites, and the organic matter content gradually decrease, while the terrigenous silica contents gradually increase, accompanied by the gradual development of sandy laminae.

(2) The changes in the shale types in the Wufeng Formation-Member L1 are characterized by multiple depositional cycles in the vertical direction, with strong heterogeneity and an obvious tripartite character. From bottom to top, the shales are sequentially clay shales, mixed clay-siliceous shales, siliceous shales, mixed clay-siliceous shales, and clay shales. In the lateral directions, due to the continuous collision and amalgamation between the Cathaysia Block and the Yangtze Platform, the siliceous shales gradually thicken to the north and northwest, and their last depositional cycle gradually ends at later time.

(3) In the Late Ordovician–Early Silurian, the depositional paleoenvironments can be divided into six evolutionary stages (A–F) from early to late in the study area. Stages A and F correspond to the initial stage of the platform-to-shelf transition and the period of continuous tectonic uplift, respectively. These two stages are characterized

by shallow depositional water bodies, oxygen-rich bottom water, high terrigenous inputs, and low paleoproductivity, with a predominance of clay shale deposits. Stages B, C, and D correspond to preglacial, glacial, and postglacial periods, respectively. These three stages are characterized by deep depositional water bodies, anoxic bottom water, low terrestrial inputs, and high paleoproductivities, with a predominance of siliceous shale deposits. Moreover, the TOC content decreases in the order of stage C > stage D > stage B, which was mainly due to the different degrees of water restriction. Stage E corresponds to the deposition of mixed clay-siliceous shales, and the depositional environment was between those of the siliceous shales and the clay shales.

Acknowledgements: This study was supported by the National Science and Technology Major Project (Grant No. 2017ZX05035001-002), and Excellent young and middle-aged scientific and technological innovation team project of colleges and universities in Hubei Province (Grant No. T201905), and the Natural Science Foundation of Hubei Province (Grant No. 2018CFB330 and 2016CFB601).

Author contributions: Junjun Shen performed the data analyses and wrote the manuscript. Decheng Chen contributed significantly to analysis and manuscript preparation. Konquan Chen contributed to the conception of the study. Pengwan Wang helped perform the analyses of shale types development and distribution characteristics. Dongtao Zhang helped perform the analyses of sedimentary characteristics of the different rock types. Junjun Li helped perform the analyses of depositional evolution models for the different shale types. Quansheng Cai helped perform the analyses of analysis of the sedimentary environments of the different rock types. Jianghui Meng helped perform the analysis with constructive discussions.

Conflict of interest: Authors state no conflict of interest.

References

[1] Chen L, Lu YC, Jiang S. Heterogeneity of the Lower Silurian Longmaxi marine shale in the southeast Sichuan Basin of China. Mar Pet Geol. 2015;65:232–46.
[2] Lazar OR, Bohacs KM, Macquaker JHS. Capturing key attributes of fine-grained sedimentary rocks in outcrops, cores, and thin sections: nomenclature and description guidelines. J Sediment Res. 2015;85:230–46.
[3] Ran B, Liu SG, Sun W. Lithofacies classification of shales of the Lower Paleozoic Wufeng-Longmaxi Formations in the Sichuan Basin and its surrounding areas. China Earth Sci Front. 2016;23:96–107 (in Chinese with English abstract).
[4] Hickey JJ, Henk B. Lithofacies summary of the Mississippian Barnett Shale, Mitchell 2 T. P. Sims well, Wise Country, Texas. AAPG Bull. 2007;91:437–43.
[5] Loucks RG, Ruppel SC. Mississippian Barnett Shale: Lithofacies and depositional setting of a deep-water shale-gas succession in the Fort Worth Basin, Texas. AAPG Bull. 2007;91:579–601.
[6] Abouelresh MO, Slatt RM. Lithofacies and sequence stratigraphy of the Barnett Shale in east-central Fort Worth Basin, Texas. AAPG Bull. 2012;96:1–22.
[7] Wang GC, Carr TR. Methodology of organic-rich shale lithofacies identification and prediction: a case study from Marcellus Shale in the Appalachian Basin. Computer Geosci. 2012;49:51–163.
[8] Feng ZZ. A review on the definitions of terms of sedimentary facies. J Palaeogeography. 2020;8:321–31.
[9] Ma YQ, Fan MJ, Lu YC, Guo XS, Hu HY, Chen L. Geochemistry and sedimentology of the Lower Silurian Longmaxi mudstone in southwestern China: implications for depositional controls on organic matter accumulation. 2016;75:291–309.
[10] Wang C, Zhang BQ, Shu ZG, Lu YC, Lu YQ, Bao HY. Lithofacies types and reservoir characteristics of marine shales of the Wufeng Formation-Longmaxi formation in fuling area, the Sichuan Basin. Oil Gas Geol. 2018;39:485–97 (in Chinese with English abstract).
[11] Wu LY, Lu YC, Jiang S, Liu XF, Liu ZH, Lu YB. Relationship between the origin of organic-rich shale and geological events of the Upper Ordovician-Lower Silurian in the Upper Yangtze area. Mar Pet Geol. 2019;102:74–85.
[12] Qiu XS, Yang B, Hu MY. Characteristics of Shale Reservoirs and gas content of Wufeng-Longmaxi Formation in the Middle Yangtze Region. Nat Gas Geosci. 2013;24:1274–83 (in Chinese with English abstract).
[13] Chen XH, Zhang BM, Chen L, Zhang GT, Li PJ, Zhang M. Main geological controlling factors and enrichment pattern of shale gas reservoirs in the late ordovician–early silurian strata of yichang. West Hubei Province Acta Geosci Sin. 2018;39:257–68 (in Chinese with English abstract).
[14] Han J, Cai QS, Li Y, Li XW. Forming environment and development model of high-quality marine shale: a case of the Wufeng – Longmaxi Formations shale in Zigui-Xintan section in the Middle Yangtze region. J Palaeogeography. 2019;21:661–74 (in Chinese with English abstract).
[15] Deng MZ, He DF. The geological structure in the Dangyang area and its significance to the shale gas exploration in Yichang area. China J Chengdu Univ Technol. 2018;45:487–500 (in Chinese with English abstract).
[16] Chen KQ, Zhang DZ, Tuo XS. Relationship between geological structure and marine shale gas preservation conditions in the western Middle Yangtze Block. Nat Gas Ind. 2020;40:9–19 (in Chinese with English abstract).
[17] Fan JX, Michael JM, Chen X, Wang Y, Zhang YD, Chen Q. Biostratigraphy and geography of the Ordovician-Silurian Lungmachi black shales in South China. Sci Sin (Terrae). 2012;42:130–9 (in Chinese with English abstract.
[18] Chen X, Chen Q, Zhen YY, Wang HY, Zhang LN, Zhang JP et al. Circumjacent distribution pattern of the Lungmachian graptolitic black shale (early Silurian) on the Yichang Uplift and

its peripheral region. Science China Earth Sciences. 2018;61:1195–203 (in Chinese with English abstract).
[19] Mou CL, Ge XY, Xu XS, Zhou KK, Liang W, Wang XP. Lithofacies palaeogeography of the Late Ordovician and its petroleum geological significance in Middle - Upper Yangtze Region. J Palaeogeograp (Chin Ed). 2014;16:427–40 (in Chinese with English abstract).
[20] Mou CL, Wang XP, Wang QY, Zhou KK, Liang W, Ge XY et al. Relationship between sedimentary facies and shale gas geological conditions of the Lower Silurian Longmaxi Formation in southern Sichuan Basin and its adjacent areas. J Palaeogeograp (Chin Ed). 2016;18:457–72 (in Chinese with English abstract).
[21] Xiong GQ, Wang J, Li YY, Yu Q, Men YP, Zhou XL, et al. Lithofacies palaeogeography of the Early Paleozoic black rock series in Dabashan region and their shale-gas geological significance. J Palaeogeograp (Chin Ed). 2017;19:965–86 (in Chinese with English abstract).
[22] Liang DG, Guo TL, Chen JP, Bian LZ, Zhao Z. Some progresses on studies of hydrocarbon generation and accumulation in marine sedimentary regions, Southern China(Part 2): geochemical characteristics of four suits of regional marine source rocks, South China. Mar Orig Pet Geol. 2009;14:1–15 (in Chinese with English abstract).
[23] Zhang BM, Chen XH, Cai QS, Chen L, Zhang GT, Li PJ. Advantageous gas shale lithofacies of Wufeng Formation-Longmaxi Formation in Yichang slope field of Western Hubei Province. China. 2020;47:1–14 (in Chinese with English abstract.
[24] Li YF, Zhang T, Ellis GS, Shao D. Depositional environment and organic matter accumulation of upper ordovician–lower silurian marine shale in the upper Yangtze platform, south China. Palaeogeogr Palaeoclimatol Palaeoecol 2017;466:252–64.
[25] Liu SF, Wang P, Hu MQ, Gao TJ, Wang K. Evolution and geodynamic mechanism of basin-mountain systems in the northern margin of the Middle-Upper Yangtze. Earth Sci Front. 2010;17:14–26 (in Chinese with English abstract).
[26] Li YX, Lin JH, Long YK, Li JH, Zhang LY. Exploration prospect of gas-bearing marine mudstone-shale in Lower Palaeozoic in the central Yangtze area. China Geol Bull China. 2011;30:349–56 (in Chinese with English abstract).
[27] Li YF, Shao DY, Lv HG, Zhang Y, Zhang XL, Zhang TW. A relationship between elemental geochemical characteristics and organic matter enrichment in marine shale of Wufeng Formation-Longmaxi Formation. Sichuan Basin Acta Petrole Sin. 2015;36:1470–83 (in Chinese with English abstract).
[28] Su WB, Huff WD, Ettensohn FR. K-bentonite, black-shale and flysch successions at the Ordovician-Silurian transition, South China: possible sedimentary responses to the accretion of Cathaysia to the Yangtze Block and its implications for the evolution of Gondwana. Gondwana Res. 2009;15:111–30.
[29] Mou CL, Zhou KK, Liang W, Ge XY. Early Paleozoic sedimentary environment of hydrocarbon source rocks in the Middle-Upper Yangtze Region and petroleum and gas exploration. Acta Geol Sin. 2011;85:526–32 (in Chinese with English abstract).
[30] Wang YM, Dong DZ, Huang JL, Li XJ, Wang SF. Guanyinqiao Member lithofacies of the Upper Ordovician Wufeng Formation around the Sichuan Basin and the significance to shale gas plays, SW China. Pet Exploration Develompent. 2016;43:42–50 (in Chinese with English abstract).
[31] Lundegard PD, Samuels ND. Field classification of fine-grained sedimentary rocks. J Sediment Pertology. 1980;50:781–6.
[32] Pickering K, Stow D, Watson M. Deep-water facise, processes and models: a review and classification scheme for modern and ancient sediments. Earth-Sci Rev. 1986;23:75–174.
[33] Macquaker JHS, Adams AE. Maxinizing information from fine-grained sedimentary rocks: an inculusive nomenclature for mudstones. J Sediment Res. 2003;73:735–44.
[34] Wang YM, Wang SF, Dong DZ, Li XJ, Huang JL. Lithofacies characterization of Longmaxi Formation of the Lower Silurian, Southern Sichuan. Earth Sci Front. 2016;23:119–33 (in Chinese with English abstract).
[35] Wang YM, Li XJ, Wang H. Developmental characteristics and geological significance of the bentonite in the Upper Ordovician Wufeng-Lower Silurian Longmaxi formation in eastern Sichuan Basin, SW China. Pet Exploration Dev. 2019;46:653–65 (in Chinese with English abstract).
[36] German CR, Elderfield H. Application of the Ce anomaly as a paleoredox indicator: the ground rules. Paleoceanography. 1990;5:823–33.
[37] Wilde P, Mary S, Erdtmann BD. The whole-rock Cerium anomaly: a potential indicator of eustatic sea-level changes in shales of the anoxic facies. Sediment Geol 1996;101:43–53.
[38] Wang YM, Li XJ, Dong DZ, Zhang CC, Wang SF. Main factors controlling the sedimentation of high-quality shale in Wufeng–Longmaxi Fm. Up Yangtze Reg Nat Gas Ind. 2017;37:9–20 (in Chinese with English abstract).
[39] Jones B, Manning DAC. Comparison of geochemical indices used for the interpretation of palaeoredox conditions in ancient mudstones. Chem Geol. 1994;111:111–29.
[40] Calvert SE, Pedersen TF. Geochemistry of recent oxic and anoxic sediments: implications for the geological record. Mar Geol. 1993;113:67–88.
[41] Tribovillard N, Algeo TJ, Baudin F, Riboulleau A. Analysis of marine environmental conditions based on molybdenum–uranium covariation – applications to Mesozoic paleoceanography. Chem Geol. 2012;324–325:46–58.
[42] Canfield DE. Factors influencing or organic carbon preservation in marine sediments. Chem Geol. 1994;114:315–29.
[43] Algeo TJ, Lyons TW. Mo-total organic carbon covariation in modern anoxic marine environments: implications for analysis of paleoredox and paleohydrographic conditions. Paleoceanography. 2006;21:279–98.
[44] Algeo TJ, Rowe H. Paleoceanographic applications of trace-metal concentration data. Chem Geol 2012;324:6–18.
[45] Rowe HD, Loucks RG, Ruppel SC. Mississippian Barnett Formation, Fort Worth Basin, Texas: bulk geochemical inferences and Mo-TOC constraints on the severity of hydrographic restriction. Chem Geol. 2008;257:16–25.
[46] Algeo TJ, Kuwahara K, Sano H, Bates S, Lyons T, Elswick E, et al. Spatial variation in sediment fluxes, redox conditions, and productivity in the Permian–Triassic Panthalassic Ocean. Paleogeogr Palaeoclimatol Palaeoecol. 2011;308:65–83.
[47] Pedersen TF, Calver SE. Anoxia vs productivity: what controls the formation of organic-carbon-rich sediments and sedimentary rocks? AAPG Bull. 1990;74:454–66.
[48] Wei HY, Chen DZ, Wang JG. Organic accumulation in the lower chihsia formation (Middle Permian) of South China:

contraints from pyrite morphology and multiple geochemical proxies. Palaeogeograp Palaeoclimatol Palaeoecol. 2012;353:734–86.

[49] Lu YB, Jiang S, Lu YC, Xu S, Shu Y, Wang YX. Productivity or preservation? The factors controlling the organic matter accumulation in the late Katian through Hirnantian Wufeng organic-rich shale, South China. Mar Pet Geol. 2019;109:22–35.

[50] Yan D, Wang H, Fu Q, Chen Z, He J, Gao Z. Geochemical characteristics in the Longmaxi Formation (early silurian) of South China: implications for organic matter accumulation. Mar Pet Geol. 2015;65:290–301.

[51] Chen X, Rong J, Li Y. Facies patterns and geography of the Yangtze region, South China, through the Ordovician and Silurian transition. Palaeogeogr Palaeoclimatol Palaeoecol. 2004;204:353–72.

[52] Yan DT, Wang JG, Wang ZZ. Biogenetic barium distribution from the Upper Ordovician to Lower Silurian in the Yangtze area and its significance to paleoproductivity. J Xian Pet Univer: Nat Sci Ed. 2009;24:16–9 (in Chinese with English abstract).

[53] Rong JY, Huang B. Study of mass extinction over the past thirty years: a synopsis (in Chinese). Sci Sin Terrae. 2014;44:75–174 (in Chinese with English abstract).